ORIGINAL RESEARCH

Dual Sensitization Anti-Resistant Nanoparticles for Treating Refractory Breast Cancers via Apoptosis-Inducing

Ruijun Ju[1,2], Faliang Wu[2], Yanzhao Tian[1], Jiahao Chu[2], Xiaoming Peng[2], Xiaobo Wang[1]

[1]Pharmacy Department, the 967th Hospital of PLA Joint Logistics Support Force, Dalian, People's Republic of China; [2]Beijing Key Laboratory of Enze Biomass Fine Chemicals, Beijing Institute of Petrochemical Technology, Beijing, People's Republic of China

Correspondence: Xiaobo Wang, Pharmacy Department, the 967th Hospital of PLA Joint Logistics Support Force, Dalian, People's Republic of China, Tel/Fax +86-0411-85847131, Email wxbbenson0653@sina.com

Purpose: Current chemotherapy fails to offer a desirable efficacy in clinical treatment against breast cancer due to the extensive multi-drug resistance. In this study, we developed dual sensitization anti-resistant nanoparticles to treat refractory breast cancer, aiming to benefit from photodynamic therapy and chemotherapy.

Methods: Hyaluronic acid (HA) derivative and photosensitizer chlorin e6 (Ce6) derivative were synthesized and confirmed by mass spectrometry. These derivatives and the chemotherapy agent paclitaxel were incorporated into nanoparticles by an emulsion-solvent evaporation method. The prepared nanoparticles were characterized by dynamic laser scattering, atomic force microscopy, and high performance liquid chromatography (HPLC). The efficacy and mechanisms of the nanoparticles, both in vitro and in vivo, were investigated by flow cytometry, confocal/fluorescence microscopy, and a high-content screening system.

Results: The prepared dual sensitization anti-resistant nanoparticles were round with a diameter of ~ 100 nm, exhibiting high encapsulation efficiency for the anticancer agent paclitaxel. The nanoparticles demonstrated a robust inhibitory effect against drug-resistant breast cancer cells by enhanced uptake, synergistic effect of photodynamic therapy and chemotherapy, and apoptosis-inducing via multiple pathways. In vivo efficacy, biocompatibility and safety were further confirmed acceptable in tumor-bearing mice.

Conclusion: The prepared dual sensitization anti-resistant nanoparticles were promising to treat refractory breast cancer with a controllable treatment site and minimal side effects.

Keywords: dual sensitization anti-resistant nanoparticles, drug-resistant breast cancer, apoptosis, photodynamic therapy, synergistic effect

Introduction

Breast cancer has become the biggest threat to women's health, but current therapies cannot provide a desirable efficacy.[1] The clinical treatment failure can be mainly attributed to metastasis and multi-drug resistance.[2–4] As an essential treatment for malignant tumors, chemotherapy plays an important role in reducing the burden of tumor cells and removing residual tumor cells after surgical treatment. However, free drugs in conventional chemotherapy have no selectivity in vivo, and repeated administration of drugs in large doses will cause acquired drug resistance and severe adverse reactions, eventually leading to treatment failure.

Generally, multi-drug resistance can be classified into acquired drug resistance and endogenous drug resistance. Acquired drug resistance refers to the drug resistance produced by repeated exposure to chemotherapy drugs, which is mainly characterized by superfluous expression of ATP-binding cassette (ABC) transporters on cell membranes, including p-glycoprotein (P-gP), multi-drug resistance-associated proteins (MRPs), and the breast cancer drug resistance protein (BCRP).[5] The overexpression of these transporters leads to increased drug efflux and decreased uptake, thereby reducing the efficacy of chemotherapy. However, endogenous drug resistance exists in tumor cells or stem cells before chemotherapy, mainly caused by the overexpression of oncogene Bcl-2 family members such as Bcl-2 and Bcl-XL.[6,7]

These upregulated Bcl-2 family members alleviated the damage of chemotherapy agents, reducing cancer cells' sensitivity. Thus, chemotherapy's efficacy was compromised.

In addition to chemotherapy, photodynamic therapy has recently emerged for treating superficial cancers.[8] Photodynamic therapy utilizes a specific wavelength of light to excite photosensitizer enriched in the superficial tumor, and then the photosensitizer is activated.[9] In the presence of oxygen in the tissue, photosensitizers can produce singlet oxygen via photodynamic reactions to kill tumor cells.

Chlorin e6 (Ce6) is a promising photosensitizer and can be synthesized from chlorophyll, suggesting desirable biocompatibility. Upon irradiation by appropriate laser (660 nm), Ce6 is highly efficient in generating singlet oxygen; thus, it is suitable for developing photodynamic therapy agents for killing tumors.[10,11] Furthermore, the 660 nm laser exhibits superior tissue penetration, which can penetrate several millimeters into human tissue.[12] These features of Ce6 make it suitable for treating breast cancers alone or combined with other therapies.

Vitamin E polyethylene glycol succinate (TPGS) is a hydrophilic derivative of vitamin E, which is formed by the reaction of the carboxyl group of vitamin E succinate with the hydroxyl group of polyethylene glycol. TPGS contains both vitamin E esterophilic groups and polyethylene glycol hydrophilic long chains. It has good surfactant properties and water solubility, which can significantly increase the absorption of insoluble drugs in the gastrointestinal tract and improve bioavailability.[13] Recent studies have found that TPGS has many unique characteristics, such as absorption promoter and multi-drug resistance reverser.[14]

Hyaluronic acid (HA) is an acidic mucopolysaccharide that was first isolated from the vitreous body of the bovine eye. With its unique molecular structure and physicochemical properties, HA shows versatile physiological functions in the body, such as lubricating joints, regulating the permeability of blood vessel walls, regulating protein, and promoting wound healing.[15,16] The favorable biocompatibility indicates HA is a promising excipient in modern drug delivery systems.[17]

Paclitaxel, a natural anticancer agent, has been widely used in treating breast, ovarian, and lung cancers for decades. Paclitaxel can induce tubulin and tubulin dimer of microtubules to lose their homeostasis, influence and promote tubulin polymerization and microtubule assembly, and prevent depolymerization. Thereby, paclitaxel can stabilize microtubules and inhibit the mitosis of cancer cells. However, the hydrophobic nature of paclitaxel and emerging drug resistance greatly limited its clinical application, and novel paclitaxel formulations are still needed.[18,19]

Nano-formulations have emerged for decades to fight against cancers, including liposomes, polymersomes, and nanoparticles.[20,21] These nano-formulations could improve the bioavailability of poorly soluble drugs, long-circulated in blood stream,[22] and target the tumor site. These nano-formulations could provide an alternative to treat drug-resistant breast cancer.

In this study, we designed self-assembled nanoparticles combining photodynamic therapy and chemotherapy to treat drug-resistant breast cancers. The amphiphilic HA-α-TOS polymer was synthesized by covalently connecting hydrophobic α-tocopherol succinate (α-TOS) to the hydrophilic backbone of hyaluronic acid (HA). The photosensitizer Ce6 was coupled with TPGS$_{1000}$ to synthesize Ce6-TPGS$_{1000}$ conjugate. The α-TOS polymer was used as the hydrophobic core to construct tumor microenvironment-responsive nanoparticles. The Ce6-TPGS$_{1000}$ conjugate and chemotherapy drug paclitaxel were incorporated into the nanoparticles. The combination of photodynamic therapy and chemotherapy was expected to exert their potency in treating drug-resistant breast cancer cells.

Materials and Methods
Materials and Cells
Paclitaxel and Ce6 were purchased from Macklin Biochemical Co., Ltd. (Shanghai, China). TPGS$_{1000}$ was obtained by Energy Chemical Co., Ltd. (Shanghai, China). HA (4000 Da) and α-TOS were purchased from Yuanye Bio-Technology Co., Ltd (Shanghai, China). Roswell Park Memorial Institute 1640 (RPMI-1640) medium, PBS, trypsin–EDTA, and penicillin/streptomycin solution, fetal bovine serum (FBS) were purchased from Zhong Sheng Ao Bang Co., Ltd. (Beijing, China). Other used reagents were all commercially available and used without additional purification.

Human breast cancer MCF-7 cells were obtained from the Institute of Basic Medical Sciences, Chinese Academy of Medical Sciences (Beijing, China). Drug-resistant human breast cancer MCF-7/adr cells were obtained from the Institute of Hematology & Blood Diseases Hospital, Chinese Academy of Medical Sciences (Tianjin, China). MCF-7 and MCF-7/adr cells were cultured in RPMI-1640 medium supplemented with 10% FBS. Both cell lines were maintained in a 37°C humidified incubator with a 5% CO_2 atmosphere. MCF-7 and MCF-7/adr cells used in the experiments were in the exponential growth phase, and regular mycoplasma detection was performed to ensure no contamination.

Synthesis of HA-α-TOS and Ce6-TPGS$_{1000}$

Briefly, 0.2 mmol α-TOS was dissolved in 1mL N,N-dimethylformamide (DMF), then 0.3 mmol 1-(3-Dimethylaminopropyl)-3-ethylcarbodiimide hydrochloride (EDC) and 0.3 mmol n-hydroxysuccinimide (NHS) were added, respectively. The reaction was performed under nitrogen protection at room temperature for 12 h. 2 mmol ethylenediamine (EDA) was dissolved in ice-cold DMF and added dropwise to α-TOS reaction solution for 12 h under nitrogen protection and at room temperature. The reaction solution was dialyzed with a dialysis tube for 48 h, the unreacted components were removed, and the filtrate was freeze-dried to obtain TOS-NH$_2$. Then, 0.3 mmol HA was dissolved in formamide in a 45°C water bath, 0.6 mmol EDC and NHS were added, and activated with HA solution for 6 h. 0.6 mmol TOS-NH$_2$ dissolved in 8 mL DMF was added dropwise at a feed molar ratio of 1:2, and the reaction was slowly stirred under nitrogen protection at room temperature for 24 h. The reaction solution was precipitated with excessive cold acetone, washed with cold acetone, dissolved in water, and dialyzed with a dialysis tube for 48 h. The filtrate was collected and freeze-dried to obtain the target product HA-α-TOS.

Ce6 (0.33 mmol), TPGS$_{1000}$ (0.66 mmol), carbodiimide (DCC, 0.40 mmol), and 4-dimethylaminopyridine (DMAP, 0.006 mmol) were dissolved in 3 mL dimethyl sulfoxide (DMSO) solution and stirred for 18 h under nitrogen protection at room temperature to obtain crude products. After filtering the crude product, the filtrate was transferred to a dialysis tube and dialyzed against DMSO solution for 24 h and then against deionized water for 24 h. Then, Ce6-TPGS$_{1000}$ was obtained by freeze-drying the residual in the dialysis tube.

The obtained products were detected by laser desorption ionization time-of-flight mass spectrometry (MALDI-TOF-MS, ABI4800plus, Applied Biosystems, CA, USA).

Preparation and Characterization of Nanoparticles

Dual sensitization anti-resistant nanoparticles were constructed by an emulsion-solvent evaporation method. Briefly, 10 mg HA-α-TOS and 5 mg Ce6-TPGS$_{1000}$ were accurately weighed and dissolved in 5 mL distilled water, then vortexed and shaken for 1 min to confirm fully dissolved. Then, 1 mg paclitaxel was dissolved in 200 μL chloroform. The oil in water (O/W) emulsion was prepared by ultra-sonication for 5 min under an ice bath. The O/W emulsion was volatilized overnight by stirring slowly at room temperature. Then the crude dual sensitization anti-resistant nanoparticles were obtained. Paclitaxel nanoparticles and Ce6 nanoparticles were prepared using the same procedures by excluding the addition of Ce6-TPGS$_{1000}$ and paclitaxel, respectively.

The morphology of the prepared nanoparticles was observed using an atomic force microscope (AFM, SPI3800N series SPA-400, Tokyo, Japan). The particle size distribution and zeta potential were measured by a Nano ZS90 Zetasizer (Malvern Instruments Ltd, Malvern, UK).

The encapsulated and free paclitaxel/Ce6-TPGS$_{1000}$ were separated by dextran gel chromatography. The concentration of paclitaxel/Ce6-TPGS$_{1000}$ was determined by HPLC equipped with a UV detector (LC-20AT, Shimadzu, Kyoto, Japan). The encapsulation efficiency (EE%) was calculated using the following equation: EE% = ($W_{encapsulated}$/W_{total}) ×100%, where $W_{encapsulated}$ and W_{total} represent the amount of drug in nanoparticles and the total amount of drug, respectively.

To investigate the stability of nanoparticles, the nanoparticles were added to normal saline, and 50% FBS solution and samples were withdrawn at 0, 6, 12, 24, and 48 h, respectively. Then the particle size was monitored by the Nano ZS90 Zetasizer (Malvern Instruments Ltd, Malvern, UK).

The in vitro release rates of paclitaxel from the nanoparticles were determined by dialysis against PBS (pH 7.4) containing 10% FBS. The released paclitaxel can be measured by HPLC (LC-20AT, Shimadzu, Kyoto, Japan).

Cytotoxicity Assay

To assess the dark cytotoxicity, MCF-7 and MCF-7/adr cells were seeded in 96-well plates at a density of 5×10^3 cells per well and grown in a complete RPMI-1640 medium for 24 hours. The cells were then exposed to free paclitaxel, paclitaxel nanoparticles, Ce6 nanoparticles, and dual sensitization anti-resistant nanoparticles at different concentrations (0–50 μg/mL, in paclitaxel equivalence) for 48 hours under dark conditions.

To evaluate the photodynamic cytotoxicity, the MCF-7 and MCF-7/adr cells were seeded into 96-well plates as in the previous method. Then the cells were treated with free paclitaxel, paclitaxel nanoparticles, Ce6 nanoparticles, and dual sensitization anti-resistant nanoparticles at different concentrations (0–50 μg/mL, in paclitaxel equivalence) for 12 hours. After refreshing the culture media, the wells were irradiated at 660 nm laser (50 mW) for 10 minutes and then incubated for another 36 hours.

At the end of incubation, the culture medium was discarded. 100 μL of pre-cooled 10% trichloroacetic acid (TCA) was added to each well, and the cells were fixed in a 4°C refrigerator for at least 1h. Then, each well was washed with deionized water five times to remove trichloroacetic acid. After drying, 100 μL of 0.4% sulforhodamine B (SRB, dissolved in 1% acetic acid) was added to stain the fixed cells and placed at room temperature for 20 min. The liquid in each well was discarded and then washed with 1% acetic acid five times to remove the unbound SRB. After drying completely, 200 μL of 10 mmol/L Tris Base (pH 10.5) was added to each well to dissolve bound SRB. Each well's optical density (OD) was measured at 540 nm in a microplate reader. The survival rate (%) of cells cultured after treatment was used to evaluate the toxic effects of various nanoparticles on breast cancer cells. The percentage of cells surviving was calculated according to the following formula:

Survival rate (%)=[absorbance of treated wells (A540 nm)/absorbance of blank control wells (A540 nm)]×100.

Live/Dead Assay of Synergistic Effect

A live/dead staining assay was performed after laser irradiation treatment to visualize the photodynamic cytotoxicity. Briefly, MCF-7/adr cells were seeded in 12-well plates at a density of 1.5×10^5 cells per well and incubated in a complete RPMI-1640 medium for 24 hours. Then the cells were treated with free paclitaxel, paclitaxel nanoparticles, Ce6 nanoparticles, and dual sensitization anti-resistant nanoparticles at 50 μg/mL (in paclitaxel equivalence) for 12 hours. After replacing the culture media, the wells were irradiated at 660 nm laser (100 mW) for 10 minutes.

The cells were incubated for another 12 hours, then stained with calcein AM and ethidium homodimer-1. After 30 minutes of staining, the cells were observed by a fluorescence microscope (DMi8, Leica, Weztlar, Germany).

Cellular Uptake by MCF-7/Adr Cells

The uptake of nanoparticles in drug-resistant MCF-7/adr cells was detected by confocal laser microscopy and flow cytometry using coumarin as a fluorescence marker. In this section, nanoparticles were prepared using the same procedures by replacing paclitaxel with coumarin. Drug-resistant MCF-7/adr cells in the logarithmic growth phase were seeded into confocal dishes at a concentration of 1.5×10^5 cells/well and cultured for 24 h. Then the cells were treated with normal saline, coumarin nanoparticles, Ce6 nanoparticles, and dual sensitization anti-resistant nanoparticles at 2 μg/mL (in coumarin equivalence). After 6 h incubation, the medium in the confocal dishes was discarded, and the dishes were washed three times with PBS. The cells were counter-stained with Hoechst 33342 (2 μg/mL) for 10 min. The fluorescence intensity and distribution of coumarin in the cells were observed by a confocal microscope (FV 10i-O, Olympus, Tokyo, Japan).

MCF-7/adr cells were seeded at a density of 4×10^5 cells/well in 6-well culture plates. After 24 h incubation, the cells were exposed to normal saline, coumarin nanoparticles, Ce6 nanoparticles, and dual sensitization anti-resistant nanoparticles at 2 μg/mL in coumarin equivalence. After 1 h, 2 h, 4 h, and 8 h incubation, the cells were harvested from the plates, collected, and analyzed by a FACS Calibur™ flow cytometer (BD Biosciences, CA, USA).

Apoptosis Assay in vitro

The drug-resistant MCF-7/adr cells were seeded in 6-well plates at a density of 4×10^5 cells/well for 24 h and incubated with free paclitaxel, paclitaxel nanoparticles, Ce6 nanoparticles, and dual sensitization anti-resistant nanoparticles at 50 μg/mL

in paclitaxel equivalence for 12 hours. After replacing the culture media, the cells were irradiated with a 660 nm laser (50 mW) for 10 minutes. After 24 h incubation, the cells were stained with PI and Annexin V-Alexa fluor 488 (Invitrogen, CA, USA), according to the kit's protocol. Then the cells were analyzed by flow cytometry within 1 h (Gallios, Beckman Coulter, CA, USA).

The drug-resistant MCF-7/adr cells were seeded in 12-well plates at a density of 2×10^5 cells/well for 24 h and incubated with PBS, free paclitaxel, paclitaxel nanoparticles, Ce6 nanoparticles, and dual sensitization anti-resistant nanoparticles at 50 µg/mL in paclitaxel equivalence. After 12 h, the media were refreshed, and the cells were illuminated at a 660 nm laser (50 mW) for 10 minutes. After another 6 h incubation, MCF-7/adr cells were double-stained with Hoechst 33342 and Mitotracker Red (Invitrogen, CA, USA) and detected using the Operetta high-content screening system (PerkinElmer, MA, USA).

Apoptosis-Related Proteins Assay

The drug-resistant MCF-7/adr cells were seeded into 96-well plates. When the confluence reached 40–50%, the MCF-7/adr cells were exposed to normal saline, free paclitaxel, paclitaxel nanoparticles, Ce6 nanoparticles, and dual sensitization anti-resistant nanoparticles at 50 µg/mL in paclitaxel equivalence. After 12 h, the media were replaced by new media, and the cells were exposed to a 660 nm laser (50 mW) for 10 minutes. After another 12 h incubation, the cells were fixed by 4% paraformaldehyde, permeabilized by Triton X-100, and blocked by goat serum. Then the cells were incubated with several primary antibodies, including anti-caspase 3, anti-caspase 8, anti-caspase 9, anti-Mcl-1, anti-Bax, and anti-cytochrome c antibodies (Sangon, Shanghai, China). The cells were further stained by Alexa fluor-488-labeled secondary antibody (Invitrogen, CA, USA) and DAPI (KeyGene BioTech, Nanjing, China). The fluorescence intensity of Alexa fluor-488 in each well was recorded by the Operetta high-content screening system (PerkinElmer, MA, USA).

In vivo Efficacy of Nanoparticles

Female Nu/Nu nude mice were obtained from Beijing Vital River Laboratory Animal Technology Co., Ltd. (Beijing, China). All animal experiments were performed under ethical guidelines and approved by the Bioethics Committee of the Beijing Institute of Petrochemical Technology. Briefly, Nu/Nu female nude mice (6 weeks old) were inoculated subcutaneously with 1×10^7 MCF-7/adr cells into the right flanks. Tumor volume was measured by a digital caliper and calculated as length×width^2/2. Tumors were allowed to expand to a volume of ~ 500 mm^3 before extraction, and the obtained tumors were cut and subsequently seeded into fresh nude mice. When the tumor volume approached ~100 mm^3, the nude mice were randomly classified into five treatment groups (n = 6). The mice were injected intravenously via the tail vein with normal saline, free paclitaxel, paclitaxel nanoparticles, Ce6 nanoparticles, and dual sensitization anti-resistant nanoparticles (in 5 mg/kg paclitaxel equivalence). The tumor-bearing nude mice were administered the formulations every other day five times. The next day after injection, the Ce6 nanoparticles group and dual sensitization anti-resistant nanoparticles group received a 660 nm (100 mW) irradiation for 5 minutes. The laser spot was placed on the tumor lump. The tumor volume and mice's body weight were recorded every day. The relative ratio of tumor volume was obtained with the following formula: the relative ratio to tumor volume (%) = $V_n/V_{14} \times 100$, where V_n represents the tumor volume at day n and V_{14} refers to the tumor volume at the initial dosing day 14.

Statistical Analysis

One-way ANOVA was employed to determine the significance among groups, after which, post hoc tests with the Bonferroni correction were used for multiple comparisons between individual groups. Data were presented as mean ± standard deviation (SD).

Results
Characterizations of HA-α-TOS and Ce6-TPGS$_{1000}$

Figure 1 depicts the synthetic routes and characterization of synthesized materials HA-α-TOS and Ce6-TPGS$_{1000}$. The results from the MALDI-TOF-MS spectra of HA-α-TOS and Ce6-TPGS$_{1000}$ strongly supported the successful conjugation of the building blocks.
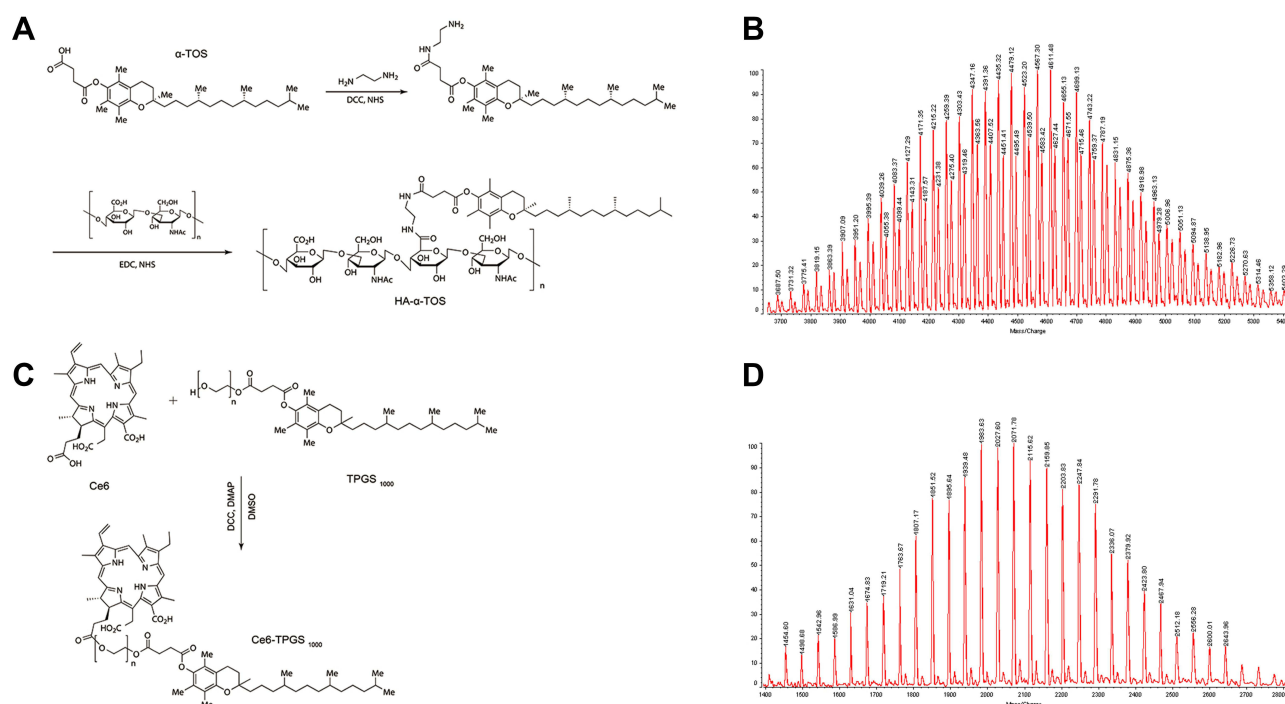
**Figure 1** Synthesis and characterization of HA-α-TOS (**A** and **B**) and Ce6-TPGS$_{1000}$ (**C** and **D**).

Characterizations of Nanoparticles

Figure 2 shows the characterizations of prepared nanoparticles. Figure 2A depicts the schematic diagram of dual sensitization anti-resistant nanoparticles. Figure 2B shows the AFM images of prepared nanoparticles. These nanoparticles were round in shape, and the diameters were ~ 80 nm for paclitaxel nanoparticles, ~100 nm for Ce6 nanoparticles, and dual sensitization anti-resistant nanoparticles. Figure 2C and D show the size distribution and zeta potential measured by dynamic laser scattering (DLS), and the raw data were summarized in Table 1. The mean size of paclitaxel nanoparticles, Ce6 nanoparticles, and dual sensitization anti-resistant nanoparticles was 68.1 ± 3.2 nm, 92.4 ± 4.3 nm, and 108.5 ± 5.5 nm, respectively. The zeta potentials of prepared nanoparticles ranged from -15.9 ± 0.4 mV to -14.3 ± 0.5 mV. The slightly negative zeta potentials may provide more extended physical stability for nanoparticles. The polydispersity index (PDI) for the prepared nanoparticles was lower than 0.25, and the small PDI indicated the homogeneity of nanoparticles. For all nanoparticles, the encapsulation efficiency of paclitaxel was >95%, and the encapsulation efficiency of Ce6-TPGS$_{1000}$ was about 80%. Figure 2E depicts the mean particle size of prepared nanoparticles in various solutions. Ce6 nanoparticles and dual sensitization anti-resistant nanoparticles had negligible mean size change, while the mean size of paclitaxel increased. Figure 2F shows the in vitro release of paclitaxel in PBS (pH 7.4). Paclitaxel nanoparticles and dual sensitization anti-resistant nanoparticles had a released rate at 48 h of $6.0 \pm 0.5\%$ and $0.5 \pm 0.1\%$, respectively. The lower release rate at 48 h could ensure the integrity of nanoparticles during drug delivery to the target site.

Cytotoxicity to Breast Cancer Cells

Figure 3 shows the cytotoxicity of various formulations to MCF-7 (Figure 3A and B) and drug-resistant MCF-7/adr cells (Figure 3C and D). The cells were treated in a dark environment (Figure 3A and C) or irradiated by a 660nm laser for 10 min (Figure 3B and D). MCF-7 cells were sensitive to the anticancer agent paclitaxel in dark conditions, while Ce6 alone showed no cytotoxicity (Figure 3A). The inhibitory effect was dose-dependent for paclitaxel formulations, and free paclitaxel had the most substantial anti-proliferation effect among paclitaxel formulations. The Ce6 nanoparticles had negligible cytotoxicity in the dark environment, indicating the favorable biocompatibility of synthesized materials.

Figure 3B shows the inhibitory effect of various formulations after 660nm laser irradiation. Free paclitaxel and paclitaxel nanoparticles exhibited comparable cytotoxicity with/without irradiation, which could be attributed to
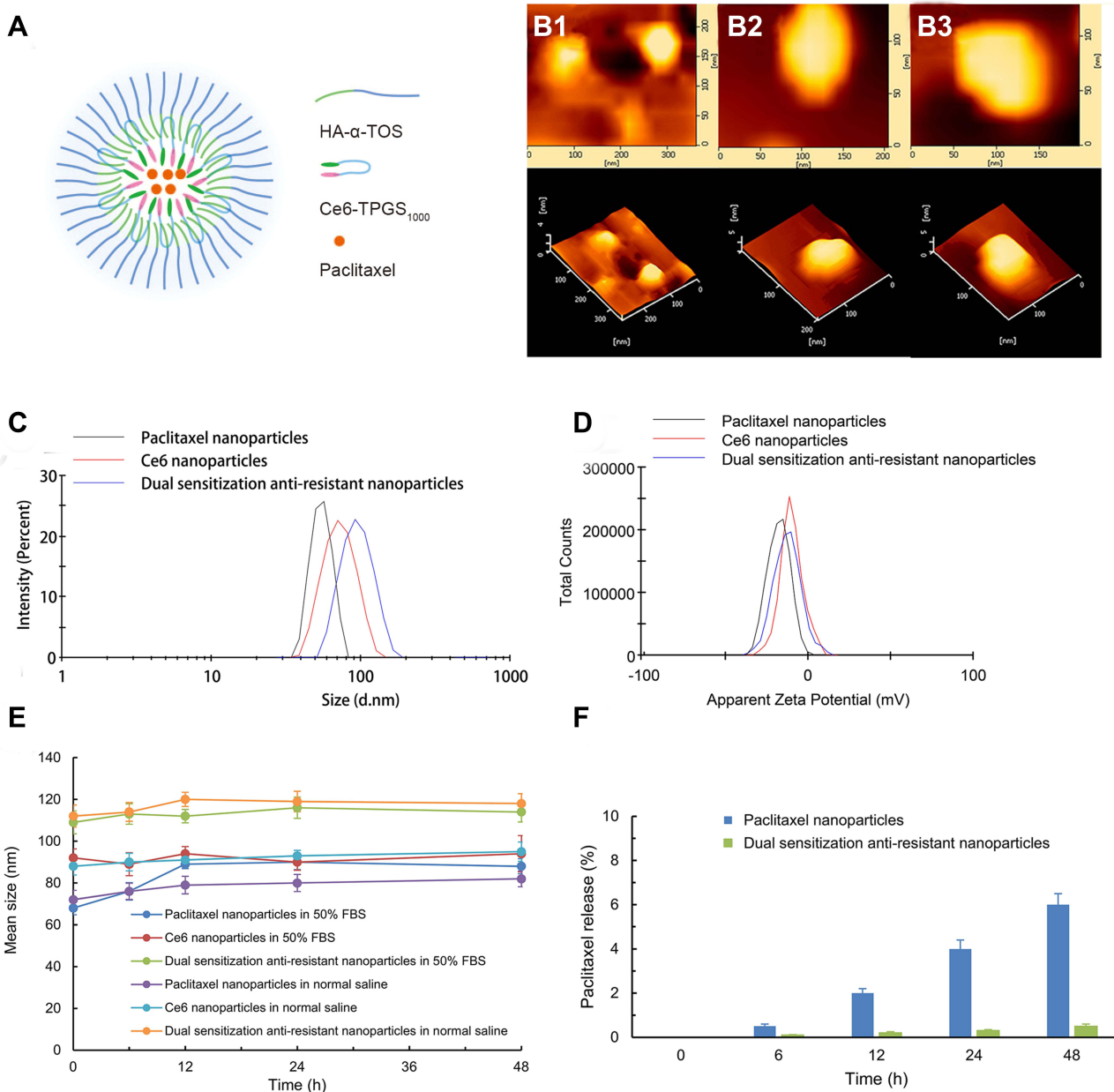
Figure 2 Characterization of prepared nanoparticles.
Notes: (**A**) Schematic diagram of dual sensitization anti-resistance nanoparticles; (**B**) AFM images of paclitaxel nanoparticles (B1), Ce6 nanoparticle (B2), and dual sensitization anti-resistance nanoparticle (B3); (**C**) the size distribution of prepared nanoparticles; (**D**) the zeta potentials of prepared nanoparticles; (**E**) mean particle size of prepared nanoparticles in normal saline and 50% FBS solution; (**F**) in vitro release of paclitaxel in PBS (pH 7.4). All the data are presented as the mean ± standard deviation (n = 3).

paclitaxel's non-sensitivity to laser exposure. However, the Ce6 nanoparticles and dual sensitization anti-resistant nanoparticles showed enhanced anticancer efficacy after irradiation. Dual sensitization anti-resistant nanoparticles also demonstrated a significant synergistic effect, combining chemotherapy with photodynamic therapy.

Figure 3C shows the dark cytotoxicity against drug-resistant MCF-7/adr cells. Unlike MCF-7 cells, MCF-7/adr cells were not sensitive to anticancer agents. All the formulations exhibited undesirable inhibitory effects against drug-resistant MCF-7/adr cells, even at the highest paclitaxel concentration (50 μg/mL).

Figure 3D shows the inhibitory effect of various formulations after 660 nm laser irradiation. The free paclitaxel and paclitaxel nanoparticles had low cytotoxicity due to the multi-drug resistance of MCF-7/adr cells. However, the Ce6

Table 1 Characterization of Prepared Nanoparticles

| Nanoparticles	Mean Size (nm)	PDI	Zeta Potential (mV)	EE (%) of Paclitaxel	EE(%) of Ce6-TPGS$_{1000}$
Paclitaxel nanoparticles	68.1 ± 3.2	0.184 ± 0.012	−15.9 ± 0.4	98.5 ± 0.3	-
Ce6 nanoparticles	92.4 ± 4.3	0.225 ± 0.023	−15.2 ± 0.6	-	82.1 ± 0.4
Dual sensitization anti-resistance nanoparticles	108.5 ± 5.5	0.237 ± 0.019	−14.3 ± 0.5	97.6 ± 0.5	78.5 ± 1.2

Note: Data are presented as the mean ± SD.
Abbreviations: PDI, polydispersity index; EE, encapsulation efficiency.

nanoparticles and dual sensitization anti-resistant nanoparticles demonstrated improved anticancer efficacy after laser exposure. Dual sensitization anti-resistant nanoparticles had the most robust anti-proliferation effect, indicating a significant synergistic effect.

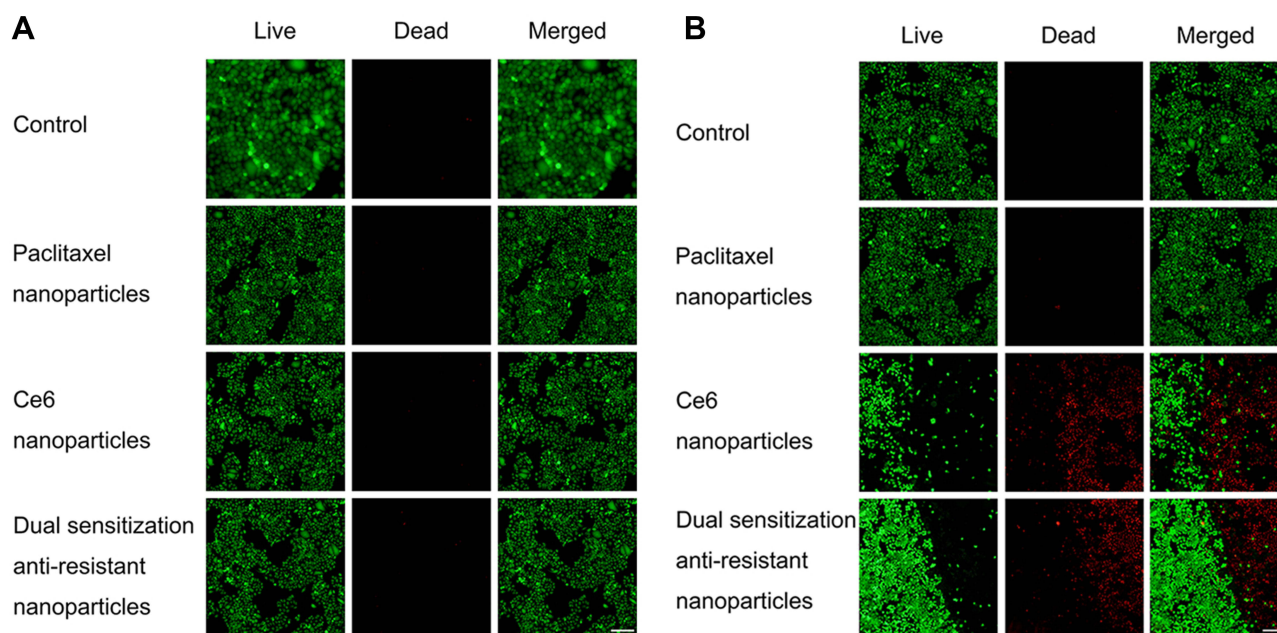## Live/Dead Assay of the Synergistic Inhibitory Effect

Figure 4 shows the survival status of drug-resistant MCF-7/adr cells after treatment with various nanoparticles in dark conditions (Figure 4A) and after laser irradiation (Figure 4B). In Figure 4A, all the MCF-7/adr cells treated with various nanoparticles grew well in dark conditions, and negligible cell death was observed. The results agreed with the negligible dark cytotoxicity of formulations against drug-resistant MCF-7/adr cells. Figure 4B demonstrates the cell status after 660 nm laser irradiation. Cells treated with paclitaxel nanoparticles exhibited little cell death, which may be attributed to the non-sensitivity to laser and multi-drug resistance. Ce6 nanoparticles and dual sensitization anti-resistant nanoparticles showed a significant cell-killing effect after 660nm laser irradiation. However, there also existed some live cells in the laser-exposed region (green cells surrounded by red cells in Figure 4B). The cells treated with dual sensitization anti-resistant nanoparticles had the fewest live cells after laser exposure, indicating the highest potency.
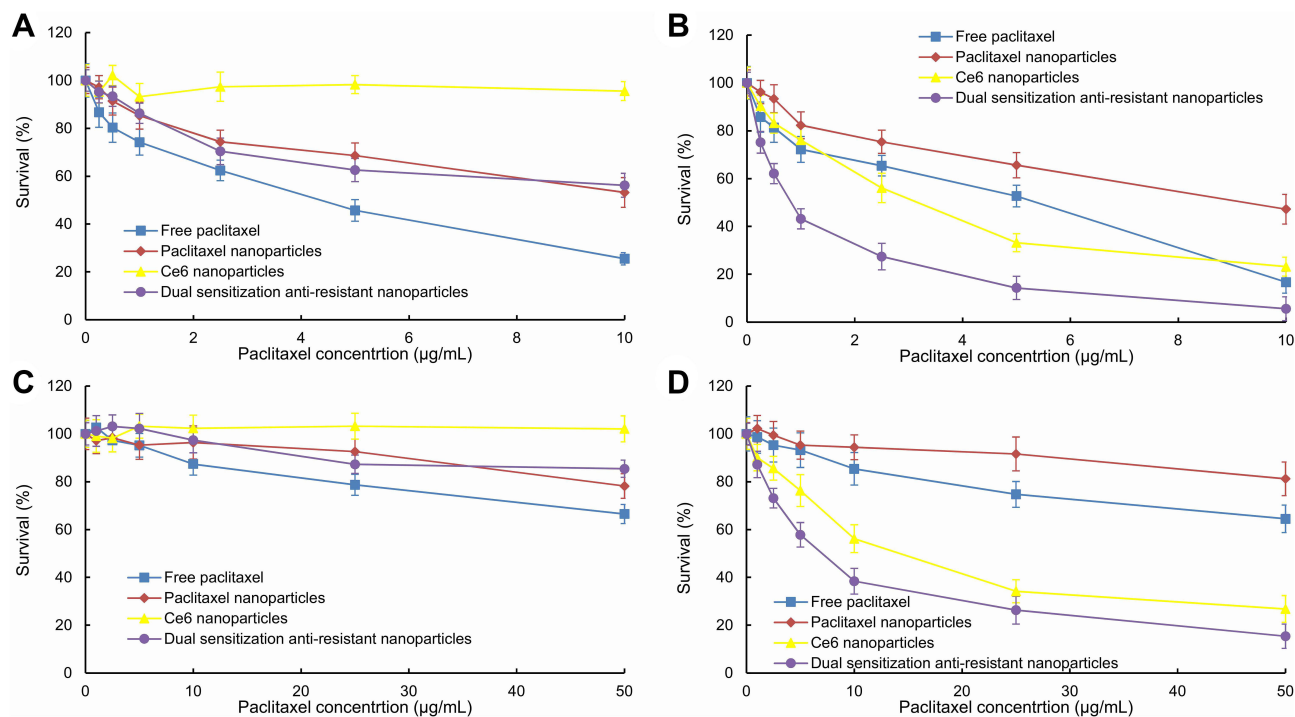
Figure 3 In vitro cytotoxic effect after treating with varying formulations.
Notes: Dual sensitization anti-resistance nanoparticles and other formulations were applied to human breast cancer MCF-7 cells (**A** and **B**) or drug-resistant human breast cancer MCF-7/adr cells (**C** and **D**) for 48 h. The cells were treated in the dark environment (**A** and **C**) or irradiated by a 660nm laser (**B** and **D**) for 10 min. Data are presented as the mean ± standard deviation (n = 6).

Figure 4 Survival status of drug-resistant MCF-7/adr cells after treatment with varying nanoparticles in dark conditions (**A**) and after laser irradiation (**B**).
Notes: The cells were observed by a fluorescence microscope. The green fluorescence indicates live cells stained by calcein AM, while the red fluorescence was emitted by the dead cells stained by ethidium homodimer. The dashed lines indicate the laser boundary. Scale bar = 200 μm.

Cellular Uptake of Various Nanoparticles

Figure 5 shows the cellular uptake of various nanoparticles labeled with coumarin. Figure 5A demonstrates the confocal images of different coumarin nanoparticles in the drug-resistant MCF-7/adr cells after treatment with coumarin nanoparticles. Cell exposed to free coumarin had minimal green fluorescence emission, indicating the internalized amount of coumarin was limited. The bright green fluorescence in the cells treated with coumarin nanoparticles and dual coumarin nanoparticles showed a superior uptake. In addition, small green spots were captured in the cells treated with coumarin nanoparticles and dual coumarin nanoparticles, suggesting these nanoparticles may be internalized via endocytosis.
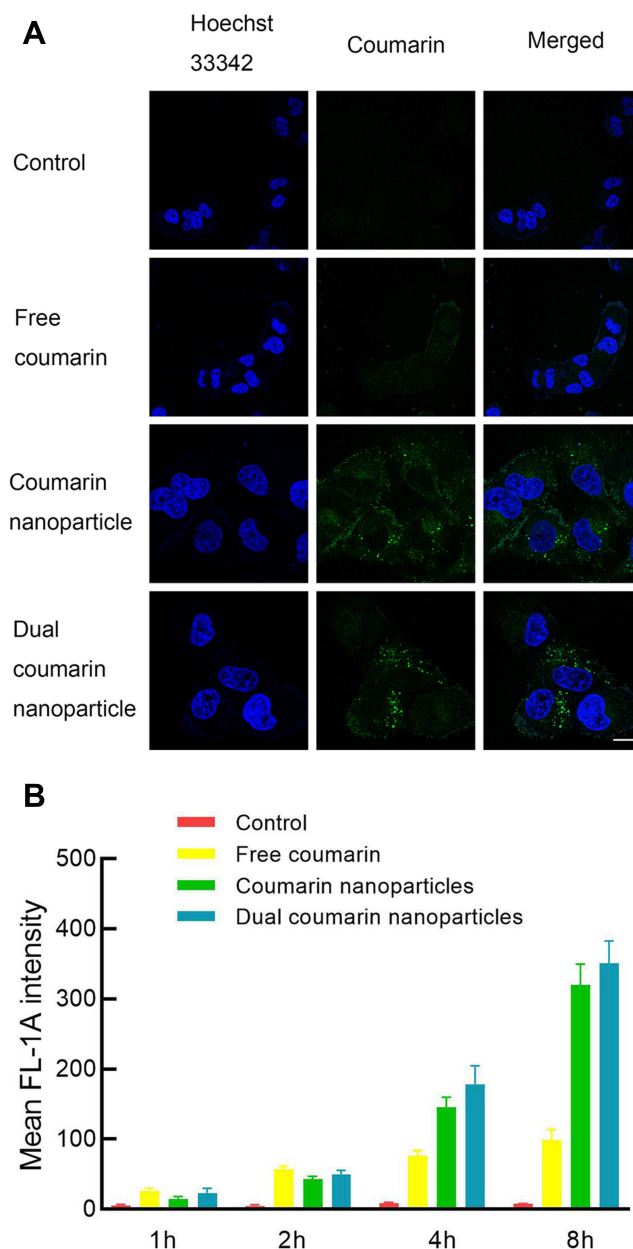
Figure 5B and Table 2 demonstrate the mean fluorescence intensity of MCF-7/adr cells after treatment with various coumarin nanoparticles for 1–8 h. Results showed that the uptake of coumarin was time-dependent, and a longer incubation time could result in more coumarin internalization. However, the uptake of free coumarin reached a plateau at 8 h, indicating a limited uptake. The uptake of coumarin nanoparticles and dual coumarin nanoparticles did not approach such a plateau, suggesting an alternative uptake mechanism. The different mechanisms may be responsible for the improved uptake of nanoparticle formulations.

Apoptosis Assay of Various Nanoparticles

Figure 6 shows the apoptosis-inducing of various nanoparticles. Figure 6A depicts the fluorescence images of the cells and their nuclei after treatment with varying formulations. Drug-resistant MCF-7/adr cells exhibited obvious cell shrinkage (shown in red fluorescence) and nuclei deformation (shown in blue fluorescence) after treatment with Ce6 nanoparticles and dual sensitization anti-resistant nanoparticles. Besides, these two treating groups had fewer cells remaining, which was consistent with the cytotoxicity of various formulations. MCF-7/adr cells showed a significant tolerance to free paclitaxel and paclitaxel nanoparticles due to multi-drug resistance.

Figure 6B illustrates the qualified apoptosis morphology data. The rank order of condensed cell percentage was dual sensitization anti-resistant nanoparticles > Ce6 nanoparticles ≈ free paclitaxel > paclitaxel nanoparticles > PBS. The rank order of nuclear fracture percentage was dual sensitization anti-resistant nanoparticles > Ce6 nanoparticles

Figure 5 Cellular uptake of various coumarin nanoparticles.
Notes: (**A**) Confocal images of various coumarin nanoparticles in the drug-resistant MCF-7/adr cells after treating with coumarin nanoparticles. Scale bar = 25 μm; (**B**) mean fluorescence intensity of drug-resistant MCF-7/adr cells after exposure to varying coumarin nanoparticles for 1–8 h.

≈ free paclitaxel > paclitaxel nanoparticles > PBS. Results showed that dual sensitization anti-resistant nanoparticles could induce the most significant morphology change during apoptosis among all formulations.

Figure 6C demonstrates the Annexin V/PI double-staining results of MCF-7/adr cells after exposure to various formulations. The apoptotic cells in the early stage can only be stained by Annexin V, yet the apoptotic cells in the late stage can be stained by both Annexin V and PI. Thus, the early apoptotic cell percentage rank order was dual sensitization anti-resistant nanoparticles > Ce6 nanoparticles ≈ free paclitaxel > paclitaxel nanoparticles > PBS. The rank order of late apoptotic cell percentage was dual sensitization anti-resistant nanoparticles > Ce6 nanoparticles > free paclitaxel > paclitaxel nanoparticles > PBS. Results showed that dual sensitization anti-resistant nanoparticles could induce the most apoptosis among all formulations.

**Table 2** Mean Fluorescence Intensity of MCF-7/Adr Cells After Various Nanoparticles' Exposure

Time (h)/Groups	Control	Free Coumarin	Coumarin Nanoparticles	Dual Coumarin Nanoparticles
1	5.6 ± 1.2	26.4 ± 3.2	14.7 ± 3.5	23.2 ± 6.7
2	4.8 ± 1.7	56.7 ± 4.6	42.7 ± 4.3	49.8 ± 5.9
4	8.4 ± 1.4	76.3 ± 7.8	145.8 ± 13.8	178.4 ± 26.3
8	7.6 ± 0.7	98.6 ± 14.8	320.4 ± 29.4	350.7 ± 32.2

Apoptosis-Related Proteins Assay

Figure 7 shows the quantitative results of apoptotic proteins in MCF-7/adr cells after various formulations exposure. After treating with normal saline, free paclitaxel, paclitaxel nanoparticles, Ce6 nanoparticles, and dual sensitization anti-resistant nanoparticles, the activity ratios of caspase 3 were 1.00 ± 0.03, 1.03 ± 0.02, 0.98 ± 0.05, 1.18 ± 0.04, 1.34 ± 0.04; the activity ratios of caspase 8 were 1.00 ± 0.04, 1.04 ± 0.01. 0.99 ± 0.06, 1.12 ± 0.03, 1.27 ± 0.03; the activity ratios of caspase 9 were 1.00 ± 0.06, 1.06 ± 0.02, 1.04 ± 0.04, 1.10 ± 0.02, 1.23 ± 0.06; the activity ratios of Bax were 1.00 ± 0.02, 1.07 ± 0.02, 1.06 ± 0.03, 1.16 ± 0.02, 1.20 ± 0.06; the activity ratios of Mcl-1 were 1.00 ± 0.04, 1.05 ± 0.03, 1.02 ± 0.04, 0.88 ± 0.04, 0.90 ± 0.04; the activity ratios of cytochrome c were 1.00 ± 0.04, 1.06 ± 0.02, 1.05 ± 0.03, 1.20 ± 0.04, 1.42 ± 0.03, respectively.
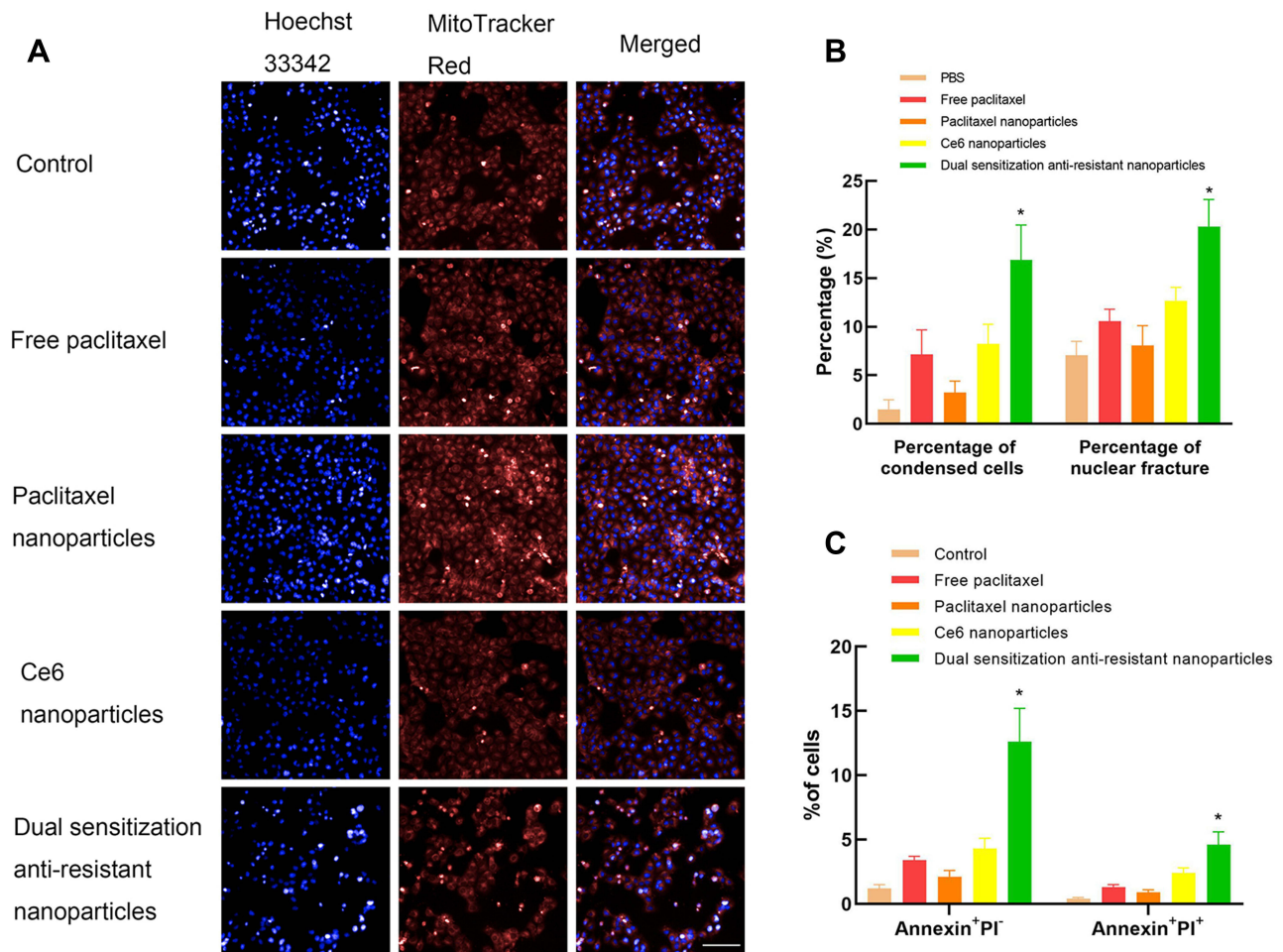
Figure 6 Apoptosis inducing of various nanoparticles.
Notes: Fluorescence images of the cells and their nuclei (**A**) were captured by a fluorescence microscope incorporated into the high-content screening system. The drug-resistant MCF-7/adr cells were stained with MitoTracker Red and Hoechst 33342 after treating with varying nanoparticles. The percentages of condensed cells and nuclear fracture (**B**) were obtained by the Columbus system. The apoptosis of MCF-7/adr cells after treatment was analyzed by flow cytometry after Annexin V/PI staining (**C**). Scale bar = 100 μm. *, $p < 0.05$ vs other formulations.
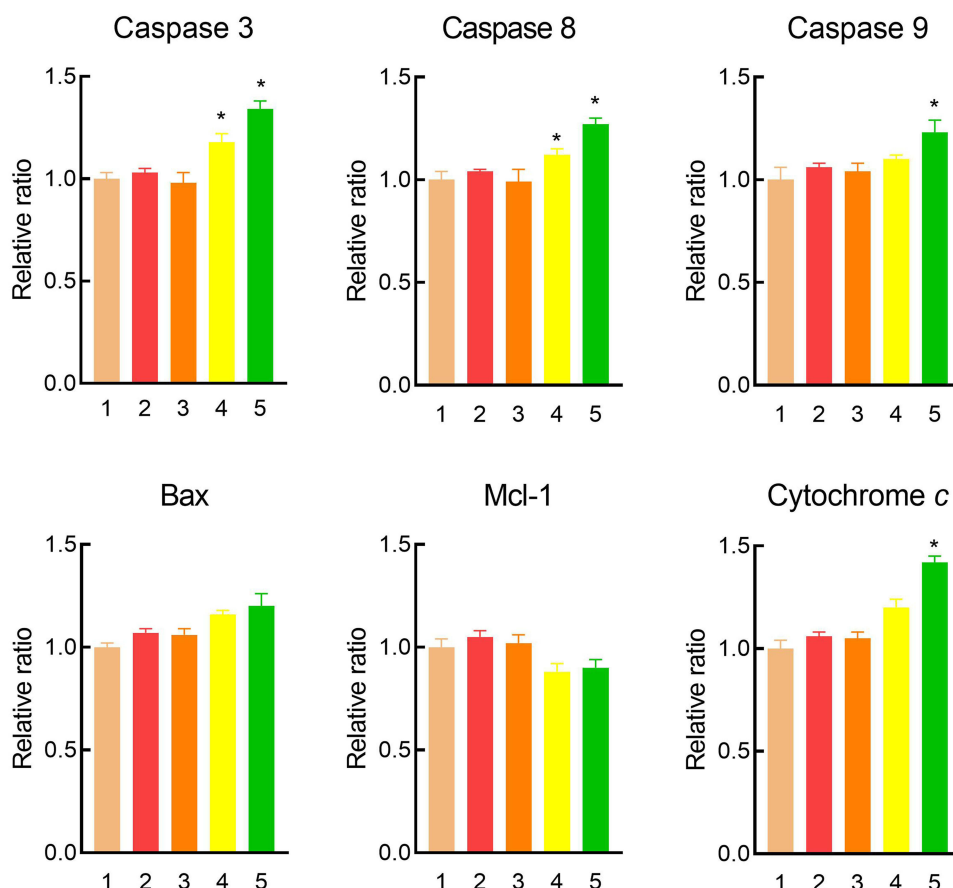
Figure 7 The changed apoptosis-related proteins of drug-resistant MCF-7/adr cells after treatment with various formulations.
Notes: The MCF-7/adr cells were treated with 1) normal saline, 2) free paclitaxel, 3) paclitaxel nanoparticles, 4) Ce6 nanoparticles, and 5) dual sensitization anti-resistant nanoparticles. Data are presented as the mean ± standard deviation (n = 3). *, $p < 0.05$ vs other formulations.

In vivo Efficacy

Figure 8 displays the tumor-bearing mice's anticancer efficacy and body weight after treatment with varying formulations. At day 24, the ranking by relative ratios of tumor volume was: normal saline < free paclitaxel < Ce6 nanoparticles < paclitaxel nanoparticles < dual sensitization anti-resistant nanoparticles (Figure 8A).
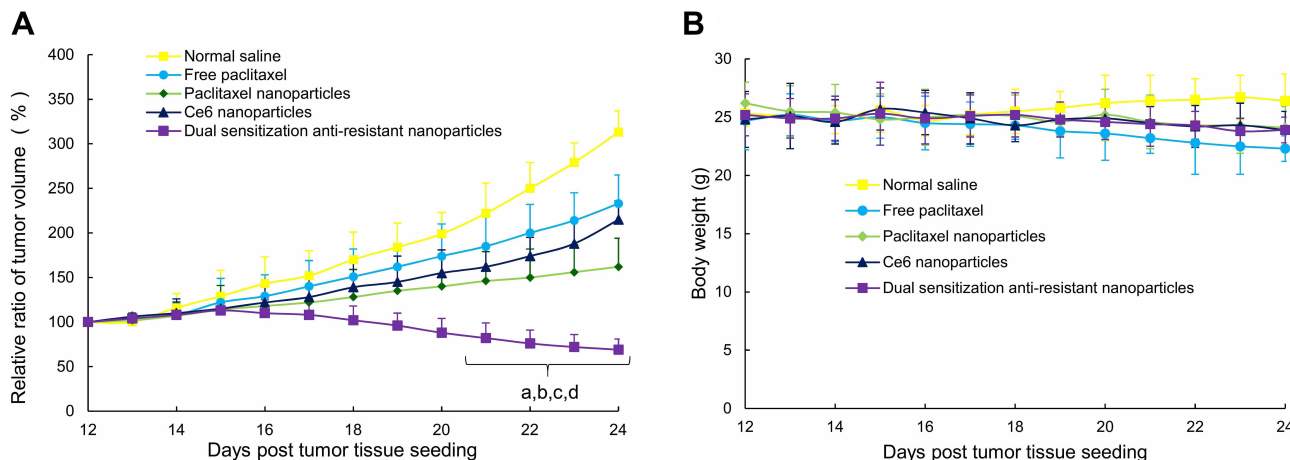
Figure 8 Anticancer efficacy (**A**) and body weight (**B**) of the tumor-bearing mice after intravenous administration of varying formulations.
Notes: Red arrows indicate the drug dosing time points. Data are presented as the mean ± standard deviation (n = 6). a, $p < 0.05$, versus normal saline; b, $p < 0.05$, versus free paclitaxel; c, $p < 0.05$, versus paclitaxel nanoparticles; d, $p < 0.05$, versus dual sensitization anti-resistance nanoparticles.

Figure 8B shows that the body weight of the tumor-bearing mice was in the range of 20–30g. However, the body weight of mice administrated with free paclitaxel dropped gradually, which may be ascribed to the organic vehicle used to dissolve the hydrophobic paclitaxel. Other nanoparticle formulations did not decrease the body weight of tumor-bearing mice, indicating satisfactory in vivo biocompatibility and safety.

Discussion

Chemotherapy has been an inevitable constituent in a comprehensive clinical strategy to treat various cancers for decades.[23–26] Despite the booming of anticancer drugs targeting novel biological targets, the efficacy of chemotherapy remains limited. The therapeutic effect of existing chemotherapy is often worse with the increase in medication time, and the clinical benefits of patients cannot meet the requirements. All the above limitations of chemotherapy are derived from multi-drug resistance, including endogenous and exogenous resistance.[27,28] In this work, we provided novel nanoparticles as a potential alternative to overcome multi-drug resistance by accumulating in tumor tissues, enhancing the uptake of nanoparticles, regulating apoptotic proteins, and inducing apoptosis.

The exogenous resistance, or acquired resistance, stems from multiple drug administrations. This results in the overexpression of ABC transporters in cell membranes that efflux chemotherapeutic drugs, leading to drug resistance.[29,30] In this work, we used paclitaxel as an anticancer agent and Ce6-TPGS$_{1000}$ as a photosensitizer to construct dual sensitization anti-resistant nanoparticles. The Ce6 was poorly soluble in aqueous media and a substrate for ABC transporters. The conjugation of Ce6 to TPGS$_{1000}$ could improve hydrophilicity and enhance solubility. Furthermore, after being degraded by enzymes in the cytoplasm, the released TPGS$_{1000}$ could serve as a multi-drug resistance reverser to inhibit the efflux of Ce6 and paclitaxel.

The prepared dual sensitization anti-resistant nanoparticles had a hydrodynamic diameter of ~100 nm, which was suitable for accumulating in tumor tissue by enhanced permeability and retention (EPR) effect.[31,32] Nano-drug delivery systems by linking target ligand molecules are often recognized and cleared by the mononuclear phagocytic system, thereby reducing the circulation time in the blood and ultimately leading to poor efficacy.[33] Alternate cationic nano-drug delivery systems can accumulate in tumor blood vessels, but they are highly toxic and easily accumulated in the liver, accelerating the clearance rate.[34] The amphiphilic Ce6-TPGS$_{1000}$, HA-α-TOS, and paclitaxel could be incorporated into the nanoparticles via hydrophobic interaction, which could be partially proven by the synergistic effect of photodynamic therapy and chemotherapy (Figure 3). It was commonly believed that stable nanoparticles had a strong zeta potential (>30 mV or < −30 mV). However, this theory only considers electrostatic repulsion, while other factors, such as van der Waals forces are ignored.[35] PEGylated nanoparticles tend to have a little net charge, but their stability is good.[36] Our nanoparticles were similar to those PEGylated nanoparticles, and their stability was further confirmed by immersing them in normal saline and 50% FBS (Figure 2E).

Results from the in vitro cytotoxicity demonstrated that MCF-7 was more sensitive to the anticancer agent than MCF-7/adr cells (Figure 3). MCF-7/adr cells were drug-resistant cells developed by multiple administrations of adriamycin. However, the drug-resistant MCF-7 cells were sensitive to photodynamic therapy. The photodynamic effect of Ce6 was triggered by 660 nm irradiation, and 10 min irradiation could significantly kill the cells. Photodynamic therapy also depends on the laser irradiation dose, so increasing the irradiation dose can dramatically improve the efficacy. The synergistic effect of photodynamic therapy combined with chemotherapy can also enhance the killing of tumor cells.

The survival status study also indicated that the synergistic killing effect could be precisely controlled. Cell killing only occurred in the laser-irradiated regions, and the dark regions exhibited negligible cytotoxicity. Thereby, side effects can be minimized.

Paclitaxel did not emit fluorescence upon irradiation, so hydrophobic coumarin was used as a fluorescence label. Coumarin was also a substrate for ABC transporters, and the efflux can be responsible for limited uptake. The decreasing fluorescence increment as incubation time increased from 1 to 8 h indicated the obvious efflux. Nanoparticles exhibited improved internalization compared with free coumarin. This phenomenon could be owing to endocytosis,[37] which was supported by the bright spots in the cytoplasm (Figure 5A). The overexpressed ABC transporters could only efflux small molecule compounds, including paclitaxel, adriamycin, and coumarin. The ABC transporter could not eliminate the

internalized nanoparticles; thus, enhanced uptake was achieved. In addition, the bright spots in the cytoplasm also suggested that the nanoparticles' integrity remained.

Apoptosis refers to the programmed death of cells after external stimulation, and different physiological changes occur in different stages of apoptosis. In the early stage of apoptosis, phosphatidyl serine (PS) turns from the inner side of the lipid membrane to the outer side, which could be detected by annexin V.[38] In the late stage of apoptosis, the integrity of the cell membrane is compromised, and the nuclei can be stained by impermeable dye PI. The cell shrinks, and the nucleus ruptures in the late apoptotic stage.[39] The apoptosis assay results indicated that dual sensitization anti-resistant nanoparticles could significantly induce cell apoptosis by a synergistic effect of photodynamic therapy and chemotherapy (Figure 6).

Apoptosis mechanisms are comprised of extrinsic and intrinsic pathways, and various proteins or enzymes are involved. Caspase 8 is the initiator in the extrinsic pathway, while Caspase 9 acts as the initiator in the intrinsic pathway. Caspase 8 and 9 activation could trigger effector Caspase 3 and then start the apoptotic cascade.[40] Bax and Mcl-1 are involved in the intrinsic pathway and serve as pro-apoptotic and anti-apoptotic proteins, respectively.[41] Cytochrome c is released once the intrinsic pathway is activated.[42] The upregulation or downregulation of the involved apoptotic proteins indicated the dual sensitization anti-resistant nanoparticles exert potency by apoptosis-inducing via multiple pathways (Figure 7). In the Bax and Mcl-1 activity ratios, dual sensitization anti-resistant nanoparticles and Ce6 nanoparticles showed statistical differences ($p<0.05$) between other groups. However, there was no statistical difference between dual sensitization anti-resistant nanoparticles and Ce6 nanoparticles, indicating photodynamic therapy might play a key role.

The anticancer study in tumor-bearing mice displayed the synergistic efficacy of the dual sensitization anti-resistant nanoparticles in treating drug-resistant breast cancer (Figure 8). The improved efficacy against exogenous resistance could be interpreted as follows: first, the dual sensitization anti-resistant nanoparticles remained stable in blood circulation; second, the proper hydrodynamic diameter of nanoparticles ensured the tumor tissue accumulation by EPR effect; third, the enhanced uptake of nanoparticles was achieved via endocytosis; fourth, the synergistic effect of photodynamic therapy and chemotherapy could be triggered by laser irradiation; and finally, nanoparticles killed the drug-resistant MCF-7/adr cells by inducing apoptosis.

Conclusions

In this study, we synthesized amphiphilic materials to construct dual sensitization anti-resistant nanoparticles to combat drug-resistant breast cancer. The prepared nanoparticles had a hydrodynamic diameter of ~ 100 nm, good stability, and minimal drug release. They could significantly improve the uptake of paclitaxel and Ce6 by drug-resistant breast cancer cells and kill the cells by a synergistic effect of combining photodynamic therapy and chemotherapy. The nanoparticles were able to induce cell apoptosis via multiple signaling pathways. Dual sensitization anti-resistant nanoparticles demonstrated potent efficacy in tumor-bearing mice. The safety and biocompatibility of the nanoparticle were favorable. The robust anticancer efficacy could be controlled by selective laser irradiation, thereby minimizing the side effects. Thus, the present study could provide a promising therapeutic strategy to surmount the multi-drug resistance in the clinical treatment of breast cancer.

Acknowledgments

Disclosure

The authors report no conflicts of interest in this work.

References

1. Fahad Ullah M. Breast cancer: current perspectives on the disease status. *Adv Exp Med Biol*. 2019;1152:51–64. doi:10.1007/978-3-030-20301-6_4
2. Kim MY. Breast cancer metastasis. *Adv Exp Med Biol*. 2021;1187:183–204. doi:10.1007/978-981-32-9620-6_9

3. Nedeljković M, Damjanović A. Mechanisms of chemotherapy resistance in triple-negative breast cancer-how we can rise to the challenge. *Cells*. 2019;8(9):957. doi:10.3390/cells8090957

4. Gote V, Nookala AR, Bolla PK, Pal D. Drug resistance in metastatic breast cancer: tumor targeted nanomedicine to the rescue. *Int J Mol Sci*. 2021;22(9):4673. doi:10.3390/ijms22094673

5. Wu Q, Yang Z, Nie Y, Shi Y, Fan D. Multi-drug resistance in cancer chemotherapeutics: mechanisms and lab approaches. *Cancer Lett*. 2014;347 (2):159–166. doi:10.1016/j.canlet.2014.03.013

6. Kartal-Yandim M, Adan-Gokbulut A, Baran Y. Molecular mechanisms of drug resistance and its reversal in cancer. *Crit Rev Biotechnol*. 2016;36 (4):716–726. doi:10.3109/07388551.2015.1015957

7. Zheng HC. The molecular mechanisms of chemoresistance in cancers. *Oncotarget*. 2017;8(35):59950–59964. doi:10.18632/oncotarget.19048

8. Champeau M, Vignoud S, Mortier L, Mordon S. Photodynamic therapy for skin cancer: how to enhance drug penetration? *J Photochem Photobiol B*. 2019;197:111544. doi:10.1016/j.jconrel.2016.06.017

9. Dolmans DE, Fukumura D, Jain RK. Photodynamic therapy for cancer. *Nat Rev Cancer*. 2003;3(5):380–387. doi:10.1038/nrc1071

10. Kumari P, Paul M, Bhatt H, et al. Chlorin e6 Conjugated Methoxy-Poly(Ethylene Glycol)-Poly(D,L-Lactide) Glutathione Sensitive Micelles for Photodynamic Therapy. *Pharm Res*. 2020;37(2):18. doi:10.1007/s11095-019-2750-0

11. Jalde SS, Chauhan AK, Lee JH, Chaturvedi PK, Park JS, Kim YW. Synthesis of novel Chlorin e6-curcumin conjugates as photosensitizers for photodynamic therapy against pancreatic carcinoma. *Eur J Med Chem*. 2018;147:66–76. doi:10.1016/j.ejmech.2018.01.099

12. Shanmugam V, Selvakumar S, Yeh CS. Near-infrared light-responsive nanomaterials in cancer therapeutics. *Chem Soc Rev*. 2014;43 (17):6254–6287. doi:10.1039/c4cs00011k

13. Choudhury H, Gorain B, Pandey M, et al. Recent advances in TPGS-based nanoparticles of docetaxel for improved chemotherapy. *Int J Pharm*. 2017;529(1–2):506–522. doi:10.1016/j.ijpharm.2017.07.018

14. Yan H, Du X, Wang R, Zhai G. Progress in the study of D-α-tocopherol polyethylene glycol 1000 succinate (TPGS) reversing multidrug resistance. *Colloids Surf B Biointerfaces*. 2021;205:111914. doi:10.1016/j.colsurfb.2021.111914

15. Bayer IS. Hyaluronic Acid and Controlled Release: a Review. *Molecules*. 2020;25(11):2649. doi:10.3390/molecules25112649

16. Abatangelo G, Vindigni V, Avruscio G, Pandis L, Brun P. Hyaluronic Acid: redefining Its Role. *Cells*. 2020;9(7):1743. doi:10.3390/cells9071743

17. Rezaei S, Kashanian S, Bahrami Y, Cruz LJ, Motiei M. Redox-Sensitive and Hyaluronic Acid-Functionalized Nanoparticles for Improving Breast Cancer Treatment by Cytoplasmic 17α-Methyltestosterone Delivery. *Molecules*. 2020;25(5):5. doi:10.3390/molecules25051181

18. Bernabeu E, Cagel M, Lagomarsino E, Moretton M, Chiappetta DA. Paclitaxel: what has been done and the challenges remain ahead. *Int J Pharm*. 2017;526(1–2):474–495. doi:10.1016/j.ijpharm.2017.05.016

19. Sofias AM, Dunne M, Storm G, Allen C. The battle of "nano" paclitaxel. *Adv Drug Deliv Rev*. 2017;122:20–30. doi:10.1016/j.addr.2017.02.003

20. Haggag Y, Abu Ras B, El-Tanani Y, et al. Co-delivery of a RanGTP inhibitory peptide and doxorubicin using dual-loaded liposomal carriers to combat chemotherapeutic resistance in breast cancer cells. *Expert Opin Drug Deliv*. 2020;17(11):1655–1669. doi:10.1080/17425247.2020.1813714

21. Haggag YA, Yasser M, Tambuwala MM, El Tokhy SS, Isreb M, Donia AA. Repurposing of Guanabenz acetate by encapsulation into long-circulating nanopolymersomes for treatment of triple-negative breast cancer. *Int J Pharm*. 2021;600:120532. doi:10.1016/j. ijpharm.2021.120532

22. Haggag YA, Abosalha AK, Tambuwala MM, et al. Polymeric nanoencapsulation of zaleplon into PLGA nanoparticles for enhanced pharmaco-kinetics and pharmacological activity. *Biopharm Drug Dispos*. 2021;42(1):12–23. doi:10.1002/bdd.2255

23. Hurwitz M. Chemotherapy in Prostate Cancer. *Curr Oncol Rep*. 2015;17(10):44. doi:10.1007/s11912-015-0468-7

24. Kim JH. Chemotherapy for colorectal cancer in the elderly. *World J Gastroenterol*. 2015;21(17):5158–5166. doi:10.3748/wjg.v21.i17.5158

25. Marsh S, Liu G. Pharmacokinetics and pharmacogenomics in breast cancer chemotherapy. *Adv Drug Deliv Rev*. 2009;61(5):381–387. doi:10.1016/j. addr.2008.10.003

26. Roett MA, Evans P. Ovarian cancer: an overview. *Am Fam Physician*. 2009;80(6):609–616.

27. Bukowski K, Kciuk M, Kontek R. Mechanisms of Multidrug Resistance in Cancer Chemotherapy. *Int J Mol Sci*. 2020;21(9):3233. doi:10.3390/ ijms21093233

28. Szakács G, Paterson JK, Ludwig JA, Booth-Genthe C, Gottesman MM. Targeting multidrug resistance in cancer. *Nat Rev Drug Discov*. 2006;5 (3):219–234. doi:10.1038/nrd1984

29. Liu X. ABC Family Transporters. *Adv Exp Med Biol*. 2019;1141:13–100. doi:10.1007/978-981-13-7647-4_2

30. Choi YH, Yu AM. ABC transporters in multidrug resistance and pharmacokinetics, and strategies for drug development. *Curr Pharm Des*. 2014;20 (5):793–807. doi:10.2174/138161282005140214165212

31. Maeda H, Wu J, Sawa T, Matsumura Y, Hori K. Tumor vascular permeability and the EPR effect in macromolecular therapeutics: a review. *J Control Release*. 2000;65(1–2):271–284. doi:10.1016/s0168-3659(99)

32. Subhan MA, Yalamarty SSK, Filipczak N, Parveen F, Torchilin VP. Recent Advances in Tumor Targeting via EPR Effect for Cancer Treatment. *J Personalized Med*. 2021;11(6):Jun. doi:10.3390/jpm11060571

33. Bao J, Zhang Q, Duan T, Hu R, Tang J. The fate of nanoparticles in vivo and the strategy of designing stealth nanoparticle for drug delivery. *Curr Drug Targets*. 2021;22(8):922–946. doi:10.2174/1389450122666210118105122

34. Kalyanaraman B, Cheng G, Hardy M, et al. A review of the basics of mitochondrial bioenergetics, metabolism, and related signaling pathways in cancer cells: therapeutic targeting of tumor mitochondria with lipophilic cationic compounds. *Redox Biol*. 2018;14:316–327. doi:10.1016/j. redox.2017.09.020

35. Bhattacharjee S. DLS and zeta potential - What they are and what they are not? *J Controlled Release*. 2016;235:337–351. doi:10.1016/j. jconrel.2016.06.017

36. Gabizon A, Martin F. Polyethylene glycol-coated (pegylated) liposomal doxorubicin. Rationale for use in solid tumours. *Drugs*. 1997;54(Suppl 4):15–21. doi:10.2165/00003495-199700544-00005

37. Oh N, Park JH. Endocytosis and exocytosis of nanoparticles in mammalian cells. *Int J Nanomedicine*. 2014;9(Suppl1):51–63. doi:10.2147/ijn.s26592

38. Crowley LC, Marfell BJ, Scott AP, Waterhouse NJ. Quantitation of apoptosis and necrosis by annexin v binding, propidium iodide uptake, and flow cytometry. *Cold Spring Harb Protoc*. 2016;2016(11):548. doi:10.1101/pdb.prot087288

39. Tengku Din TA, Seeni A, Khairi WN, Shamsuddin S, Jaafar H. Effects of rapamycin on cell apoptosis in MCF-7 human breast cancer cells. *Asian Pacific J Cancer Prevention*. 2014;15(24):10659–10663. doi:10.7314/apjcp.2014.15.24.10659

40. Shi Y. Mechanisms of caspase activation and inhibition during apoptosis. *Mol Cell.* 2002;9(3):459–470. doi:10.1016/s1097-2765(02)

41. Bruckheimer EM, Cho SH, Sarkiss M, Herrmann J, McDonnell TJ. The Bcl-2 gene family and apoptosis. *Adv Biochem Eng Biotechnol.* 1998;62:75–105. doi:10.1007/BFb0102306

42. Ow YP, Green DR, Hao Z, Mak TW. Cytochrome c: functions beyond respiration. *Nat Rev Mol Cell Biol.* 2008;9(7):532–542. doi:10.1038/nrm2434